Ferroelectric Properties and Crystal Structure of the Layered Intergrowth Phase Bi$_3$Pb$_2$Nb$_2$O$_{11}$Cl

Ardak M. Kusainova,[†] Philip Lightfoot,*[,†] Wuzong Zhou,[†]
Sergei Yu. Stefanovich,[‡] Alexander V. Mosunov,[‡] and Valerii A. Dolgikh[§]

*School of Chemistry, University of St-Andrews, Fife, KY16 9ST, United Kingdom,
Karpov Institute of Physical Chemistry, 103064 Moscow, Russia, and Chemistry Department,
Moscow State University, 119899, Vorob'evy Gory, Moscow, Russia*

The crystal structure and physical properties of Bi$_3$Pb$_2$Nb$_2$O$_{11}$Cl, a member of the Sillen–Aurivillius phase intergrowth family, have been probed using powder neutron diffraction, high-resolution transmission electron microscopy (HRTEM), second harmonic generation (SHG) tests, and alternating current impedance methods. It is shown that this compound undergoes a diffuse ferroelectric type phase transition at $T_c \sim 683$ K. Although the powder neutron diffraction data show that the crystal structure has pseudo-tetragonal symmetry (parent space group $P4/mmm$, $a_p = 3.910\,38(6)$ and $c_p = 18.8342(3)$ Å at 298 K), electron diffraction data clearly show a weak superlattice ($a_o \sim b_o \sim (2)^{1/2}a_p$, $c_o = c_p$) compatible with a reduction of symmetry to orthorhombic, analogous to that observed in the related Aurivillius phases, such as SrBi$_2$Ta$_2$O$_9$. Detailed analysis of the SHG data as a function of temperature suggests the existence of ordered polar nanodomains, compatible with the observation of "average" tetragonal symmetry in the neutron diffraction data. These observations, together with the presence of marked frequency dependence of T_c, point toward a relaxor type ferroelectric behavior. The nature of the crystal structure, namely, a regular intergrowth of Aurivillius-like and Sillen-like blocks, [M$_2$O$_2$]/[MNb$_2$O$_7$]/[M$_2$O$_2$]/[Cl] [M = Bi, Pb], has been established from both Rietveld refinement of the powder neutron data and directly from HRTEM images. The observation of ferroelectricity in this material suggests the existence of a wider family of new ferroelectrics analogous to the Aurivillius phases.

Introduction

The chemistry of layered oxides has become one of the most important fields of solid-state chemistry in recent years, largely driven by the structural and compositional flexibility of these phases and consequent opportunities for the design and control of novel physical and chemical properties, for example, ferroelectricity, ionic conductivity, and superconductivity. Among the various crystallochemical families of layered oxides, the Aurivillius phases,[1] of general composition [Bi$_2$O$_2$][A$_{n-1}$B$_n$O$_{3n+1}$], for example, SrBi$_2$Ta$_2$O$_9$ and Bi$_4$Ti$_3$O$_{12}$, have been widely studied for their unique ferroelectric properties[2,3] as well as high anionic conductivity (e.g., in the BIMEVOX family based on Bi$_4$V$_2$O$_{11}$[4]). A closely related series of layered intergrowths are the Sillen family of oxyhalides, of general composition [M$_2$O$_2$]X$_m$, where m = 1 or 2, M = Bi^{3+}, Pb^{2+}, Sr^{2+}, etc., and X is a halide.[5] Both families can be described in terms of alternation of different types of structural building blocks: fluorite-like [Bi$_2$O$_2$]$^{2+}$ layers and perovskite-like [A$_{n-1}$B$_n$O$_{3n+1}$]$^{2-}$ layers, where n is the thickness of the perovskite block, in the case of Aurivillius phases, and the same fluorite-like [Bi$_2$O$_2$]$^{2+}$ or, for example, [BiPbO$_2$]$^+$ layers interleaved between halogen layers in the Sillen phases.

It has been previously shown[6] that both structural types can be intergrown together in a regular manner to produce a new family of layered phases, nicknamed "Bipox" phases (for *bi*smuth *p*erovskite *ox*yhalide) by Ackerman.[7] These phases have general composition [M$_2$O$_2$][A$_{n-1}$B$_n$O$_{3n+1}$][M$_2$O$_2$][X$_m$] and may be designated as "AnXm" to express the number of perovskite (An) and halide (Xm) layers.

One of the main structural requirements for the existence and stability of intergrowth phases of this type is the geometrical compatibility of the unit cells of the parent phases. Therefore, in addition to the well-known "tolerance factor" argument (a function of cation size at the A and B sites) controlling the stability, the detailed crystallographic nature, and consequent physical properties of three-dimensional perovskites, further "compatibility" parameters must be taken into account in the understanding of intergrowth phases of, for example,

---

* To whom correspondence should be addressed. E-mail: pl@st-and.ac.uk.
† University of St-Andrews.
‡ Karpov Institute of Physical Chemistry.
§ Moscow State University.

(1) Aurivillius, B. *Ark. Kemi* **1949,** *1,* 499.
(2) Smolenski, G. A.; Isupov, V. A.; Agranovskaya, A. I. *Sov. Phys. Solid State* (*Engl. Transl.*) **1953,** *3,* 651.
(3) de Araujo, C. A. P.; Cuchlaro, J. D.; McMillan, L. D.; Scott, M. C.; Scott, J. F. *Nature* (*London*) **1995,** *374,* 627.
(4) Abraham, F.; Debruille-Gresse, M. F.; Mairesse, G.; Nowogrocki, G. *Solid State Ionics* **1988,** *28–30,* 529.
(5) Dolgikh, V. A.; Kholodkovskaya, L. N. *Russ. J. Inorg. Chem.* **1992,** *37,* 488.
(6) Aurivillius, B. *Chem. Scr.* **1984,** *23,* 143.
(7) Ackerman, J. F. *J. Solid State Chem.* **1986,** *62,* 92.

the Aurivillius and Bipox type, i.e., the compatibility of the perovskite block, as a whole, with the fluorite-like and halide sublayers.

An example of the effect of differing intergrown blocks on "the same" perovskite block is shown by the comparison of the Aurivillius phase $SrBi_2Ta_2O_9$[8] with the analogous Ruddlesden–Popper phase $K_2SrTa_2O_7$.[9] The tolerance factor (defined as $t = (r_A + r_O)/(2)^{1/2}(r_B + r_O)$, where r_A, r_B, and r_O are the ionic radii of A, B, and O ions, respectively[10]) for the $SrTa_2O_7$ block is 0.98; in other words, the Ta–O bonds in an ideal perovskite block of this type should be under a slight compressive stress (since $t < 1$). For $SrBi_2Ta_2O_9$ (orthorhombic, $a = 5.522$ and $b = 5.524$ Å, equivalent to a pseudo-tetragonal value of $\sim$3.905 Å), the Ta–O bonds are indeed under compression, leading to slight octahedral tilting whereas for $K_2SrTa_2O_7$ (tetragonal, $a = 3.986$ Å, i.e., considerably larger), the Ta–O bonds are under tension, due to the additional requirement to accommodate intergrowth with the much larger K^+-containing block, resulting in no octahedral tilting.

It is clear that such structural compatibility requirements and their understanding could be used to advantage in the design of new intergrowth phases with specific and tunable physical properties, for example, ferroelectricity. Hence, the requirement for structural size compatibility may lead to the distortion of particular fragments of the structures, such as rotation or tilting of octahedral units or displacements of cations off their "ideal" sites, as a consequence of the geometrical adaptation of each fragment to form the structure as a whole. Distortions of this type are known to play a pivotal role in the ferroelectric behavior of the Aurivillius phases,[11] and a detailed understanding of them as a function of composition and temperature has been recently pursued by us[12–14] and others.[8,15] It follows that if the detailed nature of both structure and properties in the more complex intergrowth phases of the Bipox series can be understood and can be related to the corresponding Aurivillius phases, then a much wider range of materials exhibiting ferroelectric behavior, with subsequent opportunities for greater tunability and control of properties, will become available.

In our previous work,[16] we have shown that the first member of the Bipox family, Bi_4NbO_8Cl (A1X1 type), does indeed possess ferroelectric properties ($T_c \sim 765$ K).

In earlier work,[6] Aurivillius described the synthesis and tentative structural characterization of the next member of this family, the A2X1 phase $Bi_3Pb_2Nb_2O_{11}$-Cl, which can be nominally represented as an inter-

growth between Sillen's $BiPbO_2Cl$ and Aurivillius' $Bi_2PbNb_2O_9$. In the present work, we investigate this phase in more detail and show that it also displays interesting ferroelectric behavior, which may be compared and contrasted with that of related known materials.

Experimental Section

Polycrystalline yellow powder with composition Bi_3Pb_2-$Nb_2O_{11}Cl$ was prepared by solid-state reaction of stoichiometric quantities of BiOCl, Bi_2O_3, Nb_2O_5, and PbO. Well-ground powder was placed in an evacuated silica tube and heated at $T = 993$ K for 18 h. Phase purity was monitored on a STOE STADI/P powder diffractometer operating in transmission mode and utilizing monochromated Cu Kα1 radiation.

Neutron Powder Diffraction. Powder neutron diffraction data were collected at 295 K on the high-flux diffractometer POLARIS at the ISIS facility (Rutherford Lab, Chilton, UK), operating in energy-dispersive (time-of-flight) mode. Approximately 5 g of the sample was placed in a cylindrical vanadium can and data were collected for 2 h. Only the "high-resolution" detector banks ($2\theta \sim 145°$) were used for subsequent Rietveld analysis, using the GSAS suite.[17]

Second Harmonic Generation Tests and Dielectric Measurements. A powder sample of $Bi_3Pb_2Nb_2O_{11}Cl$, with a small addition of poly(vinyl alcohol) (3% solution), was pressed into cylindrical pellets with a diameter of 8 mm and a thickness of 2–3 mm. The pellets were sintered at $T = 993$ K for 3–4 h in air. After being heated, all pellets were checked by X-ray diffraction, which demonstrated that the material retained its integrity under these conditions. Electrodes with an electrical resistance of 2–5Ω were put on both sides of the pellets by Pt-paste painting and annealing at 993 K. Dielectric constant and electrical conductivity were measured between 300 and 1000 K with PC-controlled AC bridges in the frequency range of 10^3–10^6 Hz. Second harmonic generation (SHG) tests were carried out in the range of 300–900 K by using a Nd/YAG solid-state laser operating at wavelength $\lambda_\omega = 1.064$ μm in the Q-switching mode with a repetition rate of 4 Hz. SHG signals at $\lambda_{2\omega} = 0.532$ μm from the polycrystalline samples were measured in reflection geometry relative to those of a standard thin powder (3 μm) α-quartz sample. A preliminary SHG test at room temperature gave a positive result, thus unambiguously testifying that under normal conditions, $Bi_3Pb_2Nb_2O_{11}Cl$ possesses a noncentrosymmetric crystal structure. Measurements of SHG intensity $I_{2\omega}$ vs temperature were carried out to 1000 K in a mode similar to that described earlier.[16]

High-Resolution Transmission Electron Microscope Study. High-resolution transmission electron microscope (HR-TEM) images and selected area electron diffraction (SAED) patterns were obtained on a JEOL JEM-2010 electron microscope operating at 200 kV. The specimen was prepared by gently grinding the powder sample and spreading it on a holey carbon film supported on a Cu grid. The HRTEM images were recorded at a magnification of 800 000$\times$.

Results and Discussion

Ferroelectric Behavior. Dielectric measurements, $\epsilon(T)$, of pelletized polycrystalline $Bi_3Pb_2Nb_2O_{11}Cl$ show distinctive maxima of the dielectric constant over a wide range of electric field frequencies, 1–1000 kHz (Figure 1). These maxima are indicative of a ferroelectric phase transition at around $T_c = 683$ K. However, these maxima are substantially broader than those observed for other Sillen–Aurivillius type ferroelectrics, Bi_4NbO_8-Cl and Bi_4TaO_8Cl, recently examined by us.[16] It is also

(8) Shimakawa, Y.; Kubo, Y.; Nakagawa, T.; Kamiyama, T.; Asano, H.; Izumi, F. *Appl. Phys. Lett.* **1999**, *74*, 1904.

(9) Crosnier-Lopez, M.-P.; Le Berre, F.; Fourquet, J.-L. *J. Mater. Chem.* **2001**, *11*, 1146.

(10) Shannon, R. D.; Prewitt, C. T. *Acta Crystallogr., Sect. B* **1969**, *25*, 925.

(11) Withers, R. L.; Thompson, J. G.; Rae, A. D. *J. Solid State Chem.* **1991**, *94*, 404.

(12) Blake, S. M.; Falconer, M. J.; McCreedy, M.; Lightfoot, P. *J. Mater. Chem.* **1997**, *7*, 1609.

(13) Hervoches, C. H.; Lightfoot, P. *Chem. Mater.* **1999**, *11*, 3359.

(14) Hervoches, C. H.; Irvine, J. T. S.; Lightfoot, P. *Phys. Rev. B* **2001**, *64*, 100102(R).

(15) Shimakawa, Y.; Kubo, Y.; Tauchi, Y.; Kamiyama, T.; Asano, H.; Izumi, F. *Appl. Phys. Lett.* **2000**, *77*, 2749.

(16) Kusainova, A. M.; Stefanovich, S. Yu.; Dolgikh, V. A.; Mosunov, A. V.; Hervoches, C. H.; Lightfoot, P. *J. Mater. Chem.* **2001**, *11*, 1141.

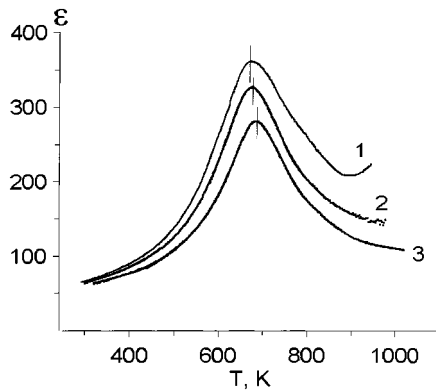(17) Larson, A. C.; Von Dreele, R. B. Los Alamos National Laboratory Report No. LA-UR-86-748, Los Alamos, NM, 1987.

Figure 1. Temperature dependence of dielectric constant ϵ for $Bi_3Pb_2Nb_2O_{11}Cl$: 1, 10 kHz; 2, 100 kHz; 3, 1 MHz.
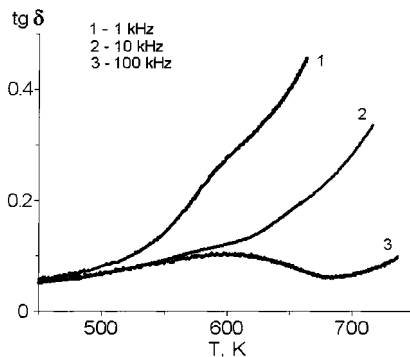
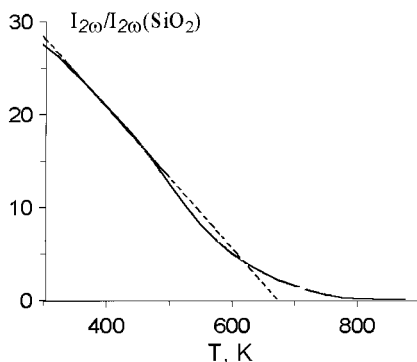**Figure 2.** Temperature dependence of dielectric loss tan δ for $Bi_3Pb_2Nb_2O_{11}Cl$: 1, 1 kHz; 2, 10 kHz; 3, 100 kHz.

Figure 3. Temperature dependence of SHG signal, relative to quartz, for $Bi_3Pb_2Nb_2O_{11}Cl$.

seen that the exact temperature of the dielectric constant maxima demonstrates a monotonic shift to higher temperature with frequency. These features of the diffuse phase transition may be attributed to some degree of structural inhomogeneity, which is probably disorder on the Bi/Pb sublattice.

Below T_c, the loss tangent demonstrates a maximum, as expected, for substances where ferroelectric domains exist. As shown in Figure 2, the tan δ maxima are smeared over a wide range of temperature below T_c in a manner similar to the $\epsilon(T)$ behavior around T_c.

SHG in Vicinity of Phase Transition. For both powdered and pelletized $Bi_3Pb_2Nb_2O_{11}Cl$ samples, second harmonic intensity gradually diminishes with temperature demonstrating no distinct anomaly at the phase transition temperature at around 683 K (Figure 3). Highlighted with a dashed line in Figure 3 is a rather rough approximation of the $I_{2\omega}(T)$ experimental curve

by a linear law from T_c toward lower temperatures, favoring a second-order phase transition for Bi_3Pb_2-$Nb_2O_{11}Cl$, by analogy with the nonsmeared ferroelectric phase transitions in Bi_4NbO_8Cl and Bi_4TaO_8Cl.[16]

In the analysis of the temperature dependence of the SHG in $Bi_3Pb_2Nb_2O_{11}Cl$ in a more strict manner, we will benefit from the fact that beyond the temperature interval of the diffuse phase transition, the $I_{2\omega}(T)$ curve does obey the usual laws for ferroelectrics with second-order phase transitions

$$I_{2\omega} \sim d^2 \sim P_s^2 \sim T_c - T \quad \text{at } T \ll T_c \qquad (1)$$

and

$$I_{2\omega} = 0 \text{ at } T \gg T_c \qquad (2)$$

According to diffuse phase transition theory summarized by Yurkevich and Rolov,[18] inside the diffuse region (denoted further as $T_c \pm \Delta T$) it is necessary to take into account a distribution of spontaneous polarization over microregions of different composition, each of them with its characteristic volume V and Curie temperature T_0. These microregions compose a system where the *averaged* value of spontaneous polarization must be calculated to account for the SHG intensity

$$I_{2\omega} \sim \langle P_s^2 \rangle \sim \int_0^{P_{max}} p^2 \exp\left\{-\frac{V\Phi(P,T)}{kT}\right\}dp \qquad (3)$$

Here, a Boltzmann type formula for the distribution of microregions over energies is used; the ferroelectric ordering energy $\Phi(P,T)$ may be expanded as

$$\Phi(P,T) = \alpha'(T - T_0)P^2 + \beta P^4 + \dots \qquad (4)$$

The notation P_{max} stands for the value of P_s at the lower-temperature boundary of the diffuse phase transition. In other words, P_{max} corresponds to the beginning of the usual linear rise of SHG when moving off the T_c region. To explore the integral, we represent the exponent as its expansion to series of only even powers of P and restrict the series by the P^4 member. Upon further replacing T_0 by its averaged value T_c and following the procedure earlier applied to diffuse phase transition examination by Rolov,[18] we come to an expression of the type

$$I_{2\omega}(T) \sim A + B(T_c - T) + C(T_c - T)^2 \qquad (5)$$

The corresponding plot is shown in Figure 4. Lines 1 and 1′ in Figure 4 represent $I_{2\omega}(T)$ behavior well below and well above the phase transition temperature T_c, with $2\Delta T$ being the temperature interval of the diffuse phase transition. Line 2 in the figure is the tangent to $I_{2\omega}(T)$ at $T = T_c$, while curve 3 represents a quadratic in the temperature contribution to SHG in the vicinity of T_c. It is seen that the non-zero value of SHG at T_c is given by the A value, the $I_{2\omega}(T)$ slope at T_c is presented by the second term $B = \tan \beta$. The third term in the series is responsible for both the SHG "tail" into the paraelectric phase as well as the deviation from linear law just below T_c. This "theoretical" curve is very close to the experimental one obtained for $Bi_3Pb_2Nb_2O_{11}Cl$.

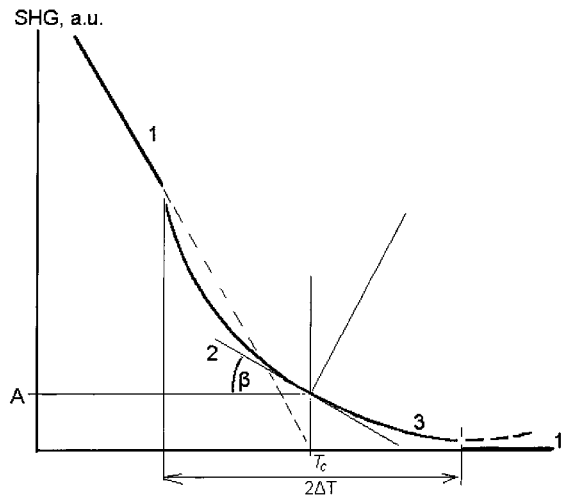(18) Yurkevich, V. E.; Rolov, B. N. *Czech. J. Phys.* **1975**, *B25*, 701.

Figure 4. Model for the SHG vs *T* behavior invoking micro-domain formation (see text).

To make numerical estimations, we note that from the thermodynamic point of view, the diffuse phenomena around the phase transition may take place if the ferroelectric-ordering energy for each microregion of volume *V* is comparable to the thermal energy ($\sim kT_c$, $k = 1.38 \times 10^{-23}$ J K^{-1} being Boltzmann's constant). Because the former is known[19] to be

$$V\Phi \approx 2\pi V \frac{\Delta T}{C} P_s^2 \tag{6}$$

the desired relation between the interval of diffusivity, $2\Delta T$, and microregion volume *V* may be obtained

$$2\Delta T = \frac{kCT_c}{\pi V P_s^2} \tag{7}$$

Here, *C* stands for the Curie−Weiss constant; P_s corresponds to the $T_c - \Delta T$ point. The value of P_s at this temperature may be evaluated from the SHG data with reference to any similar ferroelectric with known $P_s(R)$ and the $I_{2\omega}(R)$ by using the relation

$$I_{2\omega}/I_{2\omega}(R) = P_s^2/P_s^2 (R) \tag{8}$$

With the choice of $Bi_4Ti_3O_{12}$ as reference sample with $P_s(R) \sim 30$ μC cm^{-2} (according to data in ref 19) and $I_{2\omega}(R) = 400 I_{2\omega}(SiO_2)$ (our data), we have for $Bi_3Pb_2Nb_2O_{11}Cl$: $2\Delta T = 400$ K, $P_s = 6$ μC cm^{-2} at 483 K, and $T_c = 683$ K. There is some uncertainty with the Curie−Weiss constant for $Bi_3Pb_2Nb_2O_{11}Cl$, so we assume a probable value of $C = 10^3$ K to obtain a semiquantitative estimation: $V = 1.04 \times 10^{-18}$ m^3. Characteristic linear dimensions for such a region are 1 μm. Because the structural/chemical inhomogeneities have no distinct boundaries we may suppose that the most probable structural correlation length for microregions in $Bi_3Pb_2Nb_2O_{11}Cl$ is expected to be considerably smaller than this. A somewhat smaller correlation length is necessary to explain the apparent absence of macroscopic orthorhombic crystal structure distortion in the neutron experiments (see below).

(19) Lines, M. E.; Glass, A. M. *Principles and Applications of Ferroelectrics and Related Materials*; Clarendon Press: Oxford, 1977.

Table 1. Refined Structural Parameters for $Bi_3Pb_2Nb_2O_{11}Cl$ in Space Group *P4/mmm*, a = 3.910 38(6) and c = 18.8342(4) Å

atom	x	y	z	$U_{11} \times 100$	$U_{22} \times 100$	$U_{33} \times 100$
Bi1	0	0	0	3.24(9)	3.24(9)	0.7(1)
Bi2[a]	0	0	0.267 45(8)	1.58(5)	1.58(5)	2.10(9)
Bi3[a]	0.5	0.5	0.398 85(8)	0.58(3)	0.58(3)	1.94(8)
Nb	0.5	0.5	0.118 98(8)	0.21(3)	0.21(3)	0.09(5)
Cl	0	0	0.5	1.48(6)	1.48(6)	2.9(1)
O1	0.5	0.5	0	5.7(2)	5.7(2)	1.2(2)
O2	0	0.5	0.104 86(13)	0.62(7)	10.3(2)	2.9(1)
O3	0.5	0.5	0.214 87(15)	4.3(1)	4.3(1)	1.6(1)
O4	0	0.5	0.336 00(8)	0.32(5)	1.05(6)	0.97(5)

[a] Bi refined as 1/2Bi + 1/2Pb by extrapolation of scattering factors. R_{wp} = 2.75%, χ^2 = 7.3 for 1614 contributing reflections and 38 refined parameters, and *d*-spacing range 0.4 < *d* < 2.5 Å.

Crystal Structure. Aurivillius[6] suggested tentative models for $Bi_3Pb_2Nb_2O_{11}Cl$, from single-crystal X-ray data, in *Cmmm* as well as in *C4/mmm*, by using the superlattice cell $a_o \sim b_o \sim (2)^{1/2}a_p$, $c_o = c_p$, where a_p and c_p refer to the parameters used in the present model. However, since the difference in a/b parameters could not be observed and there was no deviation from *mmm* symmetry in either of these cases, both these models are essentially equivalent to the one presented below.

From our powder neutron diffraction data, no deviation of the pseudo-tetragonal cell from $a_p \sim 3.9$ and $c_p \sim 18.8$ Å could be detected. Hence, although the SHG and dielectric data clearly necessitate the adoption of a polar space group at room temparature, we chose to refine our data by using a model in the centrosymmetric tetragonal space group *P4/mmm* with a = 3.910 38(6) and c = 18.8342(1) Å; this model was found to provide a very good approximation to the true structure. In the tetragonal system, the only possible polar axis is along *c* though both the electron diffraction data presented below and previous results on Aurivillius phases suggest that the true symmetry of this phase is probably orthorhombic with $a_o \sim b_o \sim (2)^{1/2}a_p$, $c_o = c_p$, with the polar axis being in the *ab* plane.

The Rietveld analysis consisted of anisotropic refinement of the model presented in Table 1. Since Bi^{3+} and Pb^{2+} are isoelectronic they cannot be discriminated using X-ray diffraction. Moreover, the neutron-scattering lengths of Pb and Bi are also very similar (0.940 × 10^{-12} and 0.853 × 10^{-12} cm, respectively). Our preliminary refinements, however, did suggest that an improvement of fit could be obtained by the ordering of Bi/Pb over the three available sites. In the final cycles, therefore, the site occupancy of "Bi(1)" was fixed at 1.00, whereas those of "Bi(2)" and "Bi(3)" were fixed at 1.05, corresponding to random disorder of Bi/Pb over these sites. We do not, however, suggest that this ordering scheme is definitive. The large values of U_{22} for O(2) and U_{11}/U_{22} for O(1) suggest some degree of local tilting of the NbO$_6$ octahedra. This has been observed in other layered perovskites, for example, $Na_2La_2Ti_3O_{10}$,[20] where a disordered model was shown to give an improved fit. In this case, however, attempts at disordering O(2) did not improve the fit. In the final cycles, all atomic coordinates, anisotropic temperature factors, scale factor, detector zero-point, six coefficients of the background modeling function, peak profile parameter (σ_1),

(20) Wright, A. J.; Greaves, C. *J. Mater. Chem.* **1996**, *6*, 1823.

```
Bi3Pb2Nb2O11Cl  P4/mmm                                    Hist   1
Bank  2, 2-Theta   145.0, L-S cycle   63 Obsd. and Diff. Profiles
```
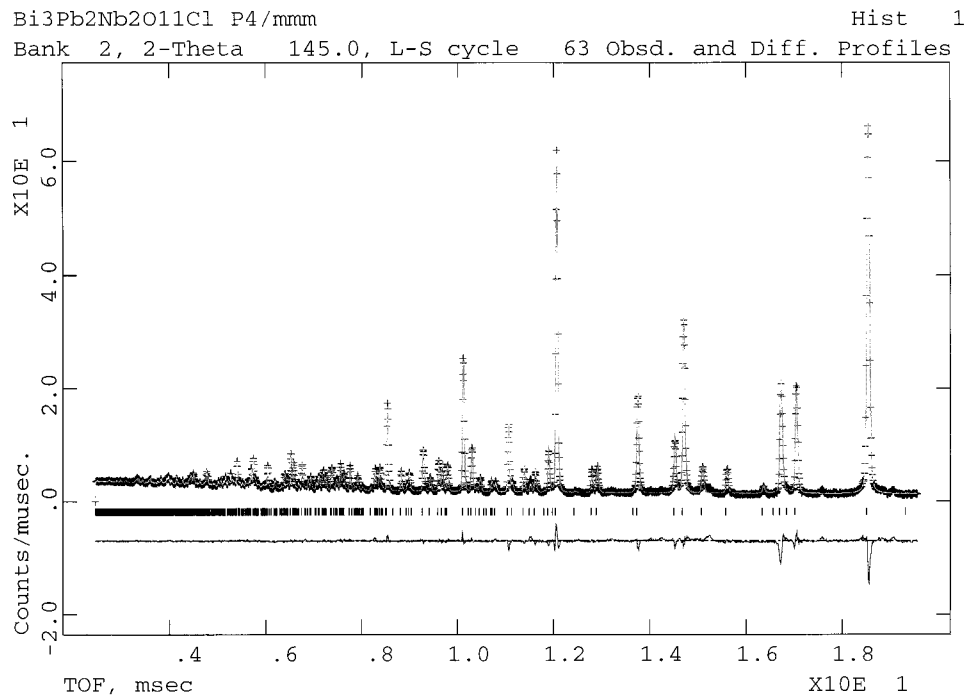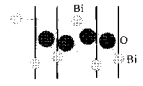

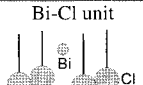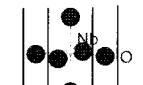**Figure 5.** Final Rietveld plot for the powder neutron diffraction refinement of $Bi_3Pb_2Nb_2O_{11}Cl$.

Table 2. Interatomic Distances for Each Atomic Site in $Bi_3Pb_2Nb_2O_{11}Cl$ and a Comparison with $Bi_2PbNb_2O_9$[23] and Bi_4NbO_8Cl[16]

	$Bi_3Pb_2Nb_2O_{11}Cl$ T_c=683K	$Bi_2PbNb_2O_9$ T_c=833K	Bi_4NbO_8Cl T_c=765K
Bi_2O_2 layer	Bi2-O3 2.937 x 4	Bi-O$_{layer}$	Bi-O
			2.21 – 3.22 (x 4) and
	Bi2-O4 2.343 x 4	2.20 - 2.41 (x 4)	2.36 – 2.94 (x 4)
		Bi-O$_{apical}$	Bi-O
	Bi3-O4 2.286 x 4		2.27 – 2.71 (x 4) and
		2.76 – 3.16 (x 4)	2.31 – 2.56 (x 4)
Bi-Cl unit	Bi3-Cl 3.358 x 4	-------	Bi-Cl
			3.25 – 3.45 (x 4) and
			3.32 – 3.39 (x 4)
NbO₆ octahedron	Nb-O1 2.241	Nb-O 2.29	Nb-O 2.05
	Nb-O3 1.806	Nb-O 1.81	Nb-O 1.96
	Nb-O2 1.973 x 4	Nb-O 1.91–2.10 x4	Nb-O 1.94 – 2.02 x 4
Bi/Pb	Bi1-O1 2.765 x 4	Pb-O	------
	Bi1-O2 2.779 x 8	2.36–3.22 x 12	

and cell parameters were simultaneously refined. Final interatomic distances are given in Table 2. Figure 5 shows the final Rietveld fit.

Our electron diffraction and HRTEM studies confirm the existence of a subtle superlattice (i.e., $(2)^{1/2}a_p \times (2)^{1/2}a_p \times c_p$) distortion of the unit cell of $Bi_3Pb_2Nb_2O_{11}$-Cl. Although these data do not definitively confirm that the true symmetry is orthorhombic, this type of superlattice is compatible with the type of distortion commonly seen in layered perovskites possessing an orthorhombic distortion. This superlattice is clearly visible in Figure 6. Detailed examination of the HRTEM image
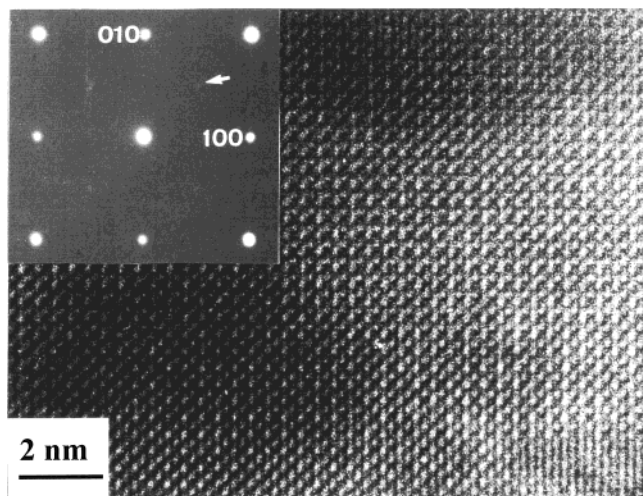
Figure 6. HRTEM image of $Bi_3Pb_2Nb_2O_{11}Cl$ viewed down the [001] direction. The inset is the corresponding SAED pattern indexed on the basic unit cell. The extra set of diffraction spots from the $(2)^{1/2} \times (2)^{1/2}$ supercell is indicated by an arrow.
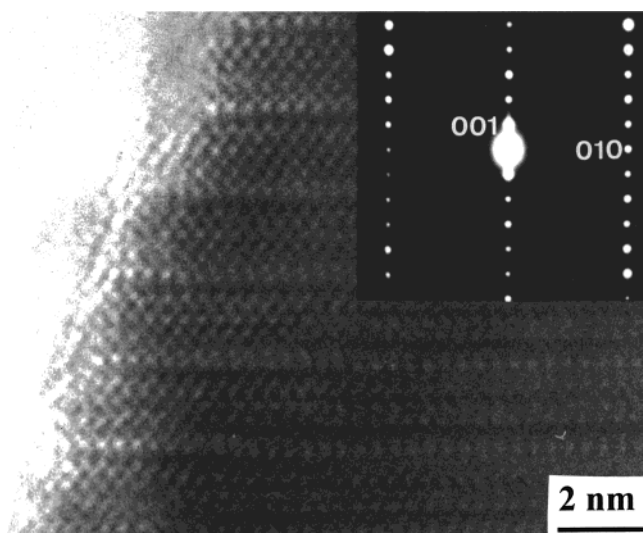

Figure 7. HRTEM image of $Bi_3Pb_2Nb_2O_{11}Cl$ viewed down the [100] zone axis of the basic unit cell. The inset is the corresponding SAED pattern, showing no superlattice or irregular layered defects along the *c*-axis.

shows a perfect intergrowth of the proposed type without any evidence of defects. In support of this, the electron diffraction patterns do not show any evidence of streaking along the *c*-axis (Figure 7). However, it should be noted that although no significant surface decomposition was observed at low magnification, at high magnification when a much higher electron beam current was applied, the existence of Cl-rich microcrystallites has been gradually observed on the particle surface by using EDX elemental analysis.

Our model of the structure of $Bi_3Pb_2Nb_2O_{11}Cl$ derived from the powder neutron data is presented in Figure 8. The structure may be described as the anticipated regular intergrowth between fluorite-like $[Bi_2O_2]$ layers, common to both Aurivillius and Sillen phases, with alternating single layers of Cl^- and double $[MNb_2O_7]$ perovskite blocks. The space group *P*4/*mmm* does not allow tilting of the NbO_6 octahedra or displacements of the Pb/Bi atoms in the perovskite A sites. These features are both observed in the well-characterized Aurivillius
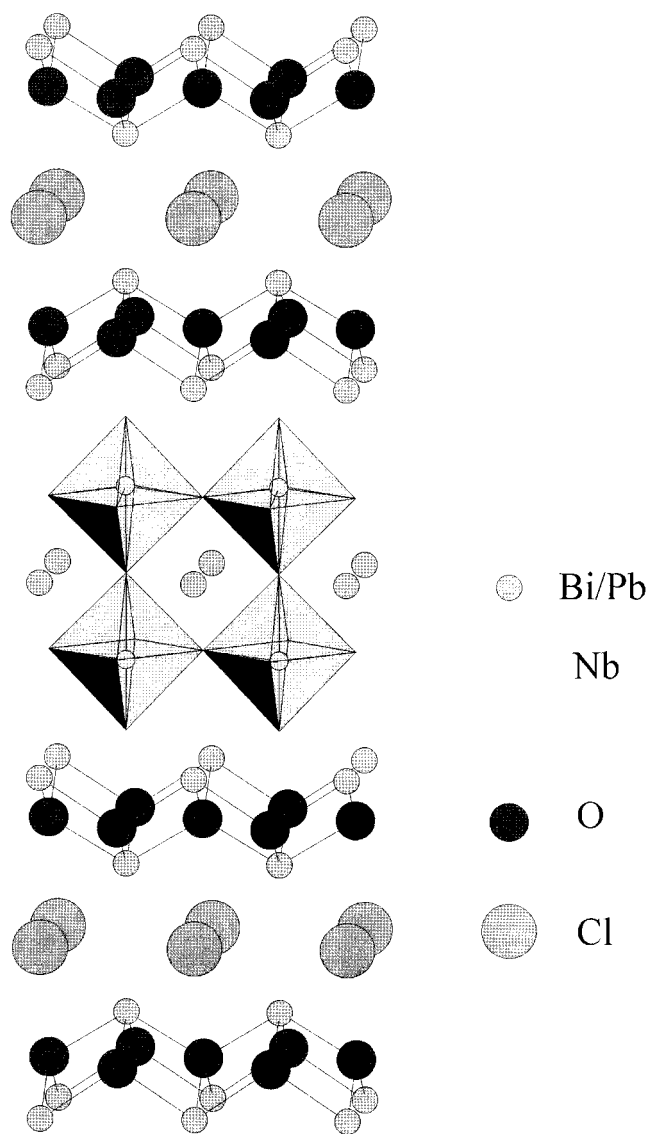

Figure 8. Ideal crystal structure of $Bi_3Pb_2Nb_2O_{11}Cl$, in space group *P*4/*mmm*.

phase ferroelectrics such as $SrBi_2Ta_2O_9$ and $Bi_4Ti_3O_{12}$. However, the electron diffraction data, together with indirect evidence from the neutron Rietveld refinement (large and anisotropic thermal parameters on O(1), O(2), and Bi(1)), suggest local displacements of atoms within the *ab* plane.

It is perhaps surprising that a macroscopic lowering of symmetry to orthorhombic cannot be seen in the neutron refinement. However, to some extent, this supports the observed peculiarities in the dielectric and SHG data, since all these techniques probe order over a wider length-scale than that studied in the electron diffraction experiment. We suggest that the TEM data set a lower limit on the microdomain size, while the SHG data impose an upper limit. Ordered nanodomains of the order of 10−100 nm are characteristic of relaxor ferroelectrics.[21] This scale is somewhat smaller than the scale suggested by our SHG measurements but is of the order required to make these features unobservable in a powder neutron diffraction experiment. A similar situation has been observed in the classic diffuse phase

(21) Ye, Z.-G. *Key Eng. Mater.* **1998**, *155−156*, 81.

transition (relaxor) ferroelectric $Pb(Mg_{1/3}Nb_{2/3})O_3$-(PMN),[22] where the crystal structure apparently remains "centrosymmetric cubic" to X-ray and neutron powder diffraction down to 5 K despite being in the ferroelectric state at these temperatures.

We have shown that $Bi_3Pb_2Nb_2O_{11}Cl$ adopts the anticipated Aurivillius−Sillen intergrowth structure ("A2X1" type) and displays relaxor type ferroelectric behavior below $T_c \sim 683$ K. A detailed examination of the crystal structure of this phase at room temperature suggests that it does not display a macroscopic lowering of symmetry from the parent tetragonal structure that is observable by powder diffraction methods. However, electron diffraction data do show a lowering of symmetry to the expected $a_o \sim b_o \sim (2)^{1/2}a_p$, $c_o = c_p$ superlattice. This may suggest that the polarization vector in the ferroelectric phase lies in the ab plane, in common with the Aurivillius phases; however, we cannot rule out the possibility of a polarization contribution along the c-axis from this study. A detailed single-crystal study of $Bi_3Pb_2Nb_2O_{11}Cl$ will be required to pin-down the true crystallographic nature of the ferroelectric phase. The present behavior, i.e., lack of a macroscopic orthorhombic distortion, differs significantly from the related Aurivillius phases, and it may be suggested that this difference is due, in part, to the requirement to accommodate intergrowth with the Sillen block, which is "relatively wide" in the ab plane. The implication is that ferroelectric domains in $Bi_3Pb_2Nb_2O_{11}Cl$ are smaller than the length-scale of the neutron diffraction experiment, which may correlate with the broadened nature of the dielectric maxima and the unusual temperature dependence of the SHG data. The unexpectedly high value of T_c for the present material, considering the above crystallographic nature (cf. the related, orthorhombic materials in Table 2), suggests that further study of these intergrowth phases may yield many more new ferroelectrics, with structural features which may provide useful insights into the behavior of not only this family but also of the Aurivillius phase ferroelectrics themselves.

CM011145N

(22) Bonneau, P.; Garnier, P.; Calvarin, G.; Husson, E.; Gavarri, J. R.; Hewat, A.; Morell, A. *J. Solid State Chem.* **1991**, *91*, 350.

(23) Srikanth, V.; Idink, H.; White, W. B.; Subbarao, E. C.; Rajagopal, H.; Sequeira, A. *Acta Crystallogr., Sect. B* **1996**, *52*, 432.